Acta Oceanol. Sin., 2018, Vol. 37, No. 3, P. 80–87
DOI: 10.1007/s13131-018-1143-2
http://www.hyxb.org.cn
E-mail: hyxbe@263.net

Wave flume experiments on the contribution of seabed fluidization to sediment resuspension

ZHANG Shaotong[1, 2], JIA Yonggang[1, 2], WANG Zhenhao[1, 2], WEN Mingzheng[1, 2], LU Fang[1, 2], ZHANG Yaqi[3], LIU Xiaolei[1, 2], SHAN Hongxian[1, 2*]

[1] Key Laboratory of Shandong Province for Marine Environment and Geological Engineering, College of Environmental Science and Engineering, Ocean University of China, Qingdao 266100, China

[2] Functional Laboratory for Marine Geology and Environment, Qingdao National Laboratory for Marine Science and Technology, Qingdao 266237, China

[3] Key Laboratory of Ministry of Education for Submarine Geosciences and Prospecting Technology, College of Marine Geosciences, Ocean University of China, Qingdao 266100, China

Received 21 April 2016; accepted 18 September 2016

Abstract

Sediment resuspension is commonly assumed to be eroded from the seabed surface by an excess bottom shear stress and evolves in layers from the top down. Although considerable investigations have argued the importance of wave-induced seabed fluidization in affecting the sediment resuspension, few studies have been able to reliably evaluate its quantitative contribution till now. Attempt is made to preliminarily quantify the contribution of fluidization to resuspension using a series of large-scale wave flume experiments. The experimental results indicated that fluidization of the sandy silts of the Huanghe Delta account for 52.5% and 66.8% of the total resuspension under model scales of 4/20 and 6/20 (i.e., relative water depth: the ratio of wave height to water depth), respectively. Some previously reported results obtained using the same flume and sediments are also summarized for a contrastive analysis, through which not only the positive correlation is confirmed, but also a parametric equation for depicting the relationship between the contribution of fluidization and the model scale is established. Finally, the contribution of fluidization is attributed to two physical mechanisms: (1) an attenuation of the erosion resistance of fluidized sediments in surface layers due to the disappearing of original cohesion and the uplifting effect resulting from upward seepage flows, and (2) seepage pumping of fines from the interior to the surface of fluidized seabed.

Key words: erosion, shear stress, seepage flows, pore pressure build up, fine-grained particles, Huanghe Delta

Citation: Zhang Shaotong, Jia Yonggang, Wang Zhenhao, Wen Mingzheng, Lu Fang, Zhang Yaqi, Liu Xiaolei, Shan Hongxian. 2018. Wave flume experiments on the contribution of seabed fluidization to sediment resuspension. Acta Oceanologica Sinica, 37(3): 80–87, doi: 10.1007/s13131-018-1143-2

1 Introduction

The most widely accepted viewpoint on sediment resuspension is that sediments are eroded by currents or stirred by waves from the seabed surface and then transported to different locations by currents. The friction between sediment particles and a current velocity or wave orbital velocity provides bottom shear stresses to counterbalance with the critical shear stress (i.e., erosion threshold) of bottom materials, thus determining the entrainment of sediments by excess shear stresses (Nielsen, 2002). On the basis of this theory, considerable research results have been reasonably explained, since a sudden increase of suspended sediment concentration (SSC) was successfully observed in both field observations and flume experiments when the bottom shear stresses exceeded a critical threshold (Green, 1992; Soulsby, 1997; Van Raaphorst et al., 1998; Kim et al., 2000; Wright et al., 2001; Wang, 2003; Biron et al., 2004; Yuan et al., 2009). Even though, it is still debatable that, in their analysis, the bottom shear stress was commonly calculated from bottom boundary layer models (e.g., Grant and Madsen, 1979), which was based on the surface erosion theory itself. In this case, even the modeled excess shear stresses well corresponded to the variations of SSC, other mechanisms might be implicitly included into a representative parameter of a coupled wave-current bottom shear stress. Recently, Green and Coco (2014) argued that to explicitly account for the effect of waves on erosion rates, merits further attention.

In fact, the role of currents or waves in causing local sediment resuspension largely depends on the morphology of estuaries or bays. In a shallow water environment, waves were frequently found to contribute more significantly or dominate the entrainment of bottom sediments (e.g., van Duin and Lijklem, 1989; Paphitis and Collins, 2005; You, 2005; Danielsson et al., 2007; Bolaños et al., 2012; Zhang et al., 2016a), with the mechanisms mostly attributed to wave orbital shear stresses or wave pumping of sediments (e.g., Wolanski and Spagnol, 2003). However, coastal engineers had an early opinion that waves not

Foundation item: The National Natural Science Foundation of China under contract Nos 41272316 and 41372287; the Joint Fund of NSFC and Marine Science Research Centers of Shandong Province of China under contract No. U1606401; the Key Research and Development Program of Shandong Province of China under contract No. 2016ZDJS09A03.
*Corresponding author, E-mail: hongxian@ouc.edu.cn

only provided the orbital shear stress to cause sediment resuspension, wave-induced dynamic bottom pressure fluctuation on a compressible silty seabed would also frequently generate pore pressure build-up (e.g., Clukey et al., 1985), which destroyed the original consolidated soil granular skeleton, increased the permeability of the seabed (Mörz et al., 2007), or even detached fine particles from large aggregates (Bennett, 1977; Bennett and Faris, 1979; Seed and Rahman, 1978; Nichols et al., 1994; Ross et al., 2011). Under storm waves, pore pressure build-up might exceed the overburden (i.e., effective stress), weaken a seabed strength, thus inducing seabed fluidization (Sumer et al., 2012; Jeng et al., 2013). In this case, even weak currents may disperse the fluidized sediments (e.g., Lambrechts et al., 2010; Zhang et al., 2016b). More recently, wave-induced pore pressure build-ups were observed to have significant promoting effects on the concentration of suspended substances in wave flume experiments (e.g., Tzang et al., 2009; Jia et al., 2014).

In summary, the mechanism of wave-induced sediment resuspension seems not only controlled by the wave orbital shear stress, the contribution of the pore pressure build-up (seabed fluidization) might also be worthy of consideration under certain circumstance. Therefore, in the present study, a series of controlled large wave flume experiments were conducted to evaluate the contribution of wave-induced seabed fluidization to sediment resuspension using the Huanghe River sandy silts. A better understanding into the physical mechanisms of silty sediment resuspension was expected. In addition, we hope the quantitative evaluation results could provide some implications for the monitoring, prediction and prevention of the active geo-hazards in the subaqueous Huanghe Delta in China.

2 Materials and methods

2.1 *Experimental setup*

Experiments were conducted in a large-scale "T" shape wave flume (Fig. 1), which primarily consists of a water flume (top of the "T") and a sediment tank (bottom of the "T"). A plywood beach, with a slope of 1:4 covered with a foam rubber of 2 cm in thickness, is located at the end of the water flume as a wave absorber. A vertical paddle which could move horizontally as a wave maker, is located at the other end of the water flume, driven by an engine with variable frequency. In this case, a wave generator pushes the wave paddle at a certain frequency to generate periodic progressive waves passing over the underlying seabed in the sediment tank. Wave parameters can be changed by controlling the driving frequency.

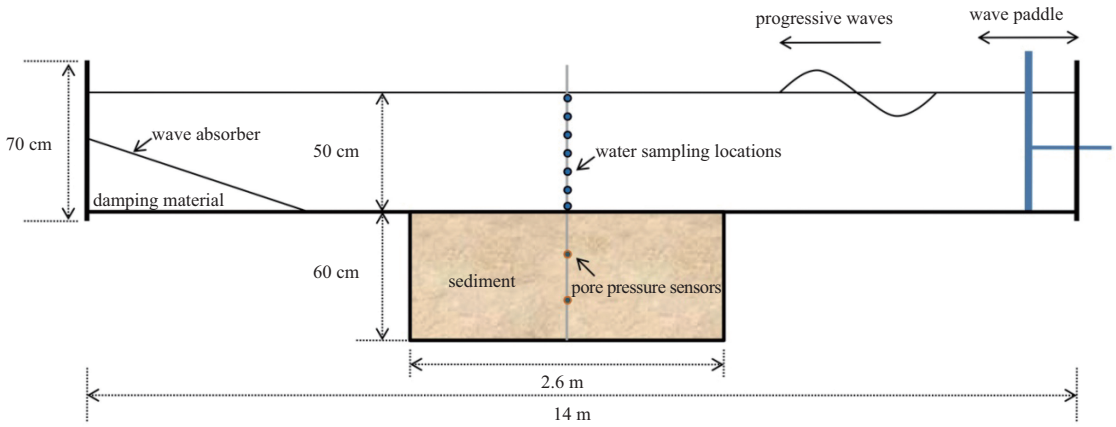

Fig. 1. Large-scale wave flume in College of Environmental Science and Engineering, Ocean University of China. The dimension of the upper water flume and the bottom sediment tank are 14 m×0.7 m×0.4 m and 2.6 m×0.6 m×0.4 m (L×H×W), respectively. The wave generator is located at the right end of the water flume, and the wave absorber is located at the left end.

2.2 *Sediment characteristics*

Experimental sediments (sandy silts) were sampled from an abandoned intertidal flat (Diaokou lobe, deposited during 1961–1976) of the modern Huanghe Delta (since 1855). A silt content ranges from 83.1% to 84.3%, a clay content ranges from 15.6% to 16.7% and a sand content ranges from 0.1% to 0.2%, with a median particle size of 43 μm. Sediment and water were well-mixed at a constant proportion of 1:4 in mass to make a slurry with a saturated water content of approximately 25% and subsequently backfilled into the sediment tank to simulate a homogeneous seabed of 0.5 m in thickness. This procedure was employed in order to simulate the rapid sedimentation process of the Huanghe River derived sediments. Because it was reported that more than 70% of the Huanghe River sediment discharge deposited within the scope of 30 km from the estuary (Bornhold et al., 1986; Saito et al., 2001), which indicated that as a huge amount of river-laden sediments flowed into the sea, a relatively homogeneous freshly-deposited seabed with a certain thickness would form due to the same deposition time. After the backfilling of the slurry, deposits were left for gravity consolidation for 4 d, then water flume was filled with water to a depth of 50 cm for further consolidation of additional 24 h under hydrostatic water pressure (i.e., wave actions commenced after 5 d since the initial deposition of the slurry, when the pore water pressure tends to be stable). Seabed preparation in both wave rounds was exactly identical.

2.3 *Suspended sediment load*

Suspended sediment load represented the total mass of suspended sediments in the whole water flume, which was measured through stratified water sampling. Seven flexible plastic pipes were vertically mounted at the centerline of the water flume with a separation distance of approximately 5 cm, with one end in the water column and the other end out of the flume. Wa-

ter samples at different depths were extracted into sample bottles by applying a negative pressure onto the outer end. Water extraction was conducted once per hour throughout both wave rounds. The turbidity of these turbid liquid samples was immediately measured using a portable turbid-meter. The turbidity was converted into concentration by the following calibration formula:

$$c_{re} = 0.004\ 09\ t + 0.512\ 49, \tag{1}$$

where c_{re} is the reference concentration (g/dm^3); and t is the water turbidity (NTU).

The conversion formula was derived from a calibration experiment. A sequence of turbid liquids with stepwise increased concentrations were prepared by adding different mass of sediments into a constant volume of water; the turbidity was also measured using the portable turbid-meter, thus the turbidity-concentration conversion formula was deduced via linear regression (Fig. 2). As r^2 was 0.965 5, we believe the conversion is reliable enough to estimate the SSC with accuracy.

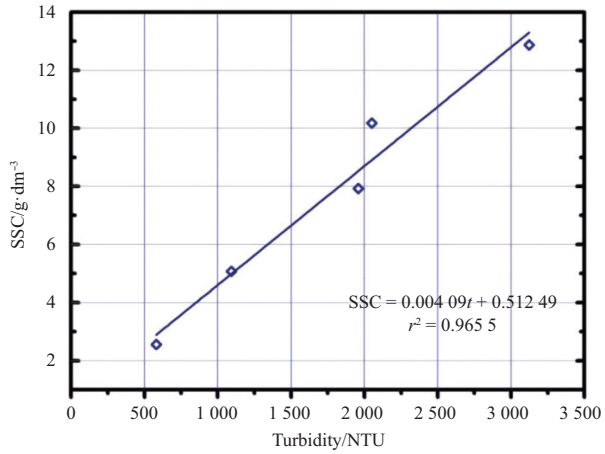

Fig. 2. Conversion formula from water turbidity to SSC derived from the calibration experiment.

The basic assumption of the stratified water sampling method is that SSC at the same elevation in the water flume can be represented by the reference concentration of the extracted water samples, i.e., when water samples are extracting, the concentration of this water layer is assumed to be horizontally uniform. Therefore, the total suspended sediment load (L_s) was estimated using the following equation:

$$L_s = A\sum_{z=1}^{n} C_z H_z\ (n=7), \tag{2}$$

where A=L×W=140×4=560 (dm^2) is the volume amplification coefficient in which L and W refer to length (dm) and width (dm) of the water flume, respectively; and C_z is the reference concentration (g/dm^3) of the water sample, z is sequence number of the water layers; H_z=0.05 is the thickness (dm) of water stratification.

2.4 *Experimental process*

Two wave rounds of 10 and 15 cm in wave height (H_w) were separately loaded on the respective seabed until the SSC finally attained an equilibrium state. Extraction of water samples and recording of fluidization depth were synchronously conducted once per hour throughout each wave rounds. Detailed information of wave parameters and loading time were summarized in Table 1.

Table 1. Wave parameters

M_s	H_w/D	T_w/s	λ/m	T_l/min	T_s/h
1.0/5.0	4/20	1.20	2.00	780	12
1.5/5.0	6/20	0.95	1.65	600	12

Note: Model scale (M_s) is the ratio of wave height (H_w) to water depth (D); T_w is the wave period; λ is the wave length; T_l is the loading time of waves; and standing time (T_s) refers to the hydrostatic settlement period after the termination of wave action.

For better understanding of the whole experimental process, typical photographs during each subperiod were arranged orderly in Fig. 3, in which the first (Fig. 3a) is a consolidation period during which pore water and bubbles were observed to be slowly extruded; Fig. 3b is the response of seabed during the 10 cm wave action and re-settled floating mud after wave termination; and Fig. 3c is the typical response of seabed during the 15 cm wave action and floating mud formed after the termination of waves. Seabed fluidization occurred in both rounds after different cycles of waves whereas the shape and size of the fluidized zone were found to be different.

3 Results

As the wave-induced seabed fluidization occurred in both rounds of the experiment, two different substages, namely before and after fluidization were divided in each round, respectively. Different characteristics in the phenomenon of fluidization, the pore pressure and SSC evolutions were detected both between the substages and the two rounds.

3.1 *Experimental phenomena*

The most representative phenomenon of seabed fluidization in the wave flume is the oscillatory motion of sediments upon a subbottom arc-shaped sliding interface. So far there is no general agreement that whether the sediment oscillation phenomenon is seabed fluidization or wave-induced shear failure. Therefore, after carefully analyzing the experimental phenomena and pore pressure data in the present study, an improved opinion on this issue was given in Section 3.3. Before this section the phenomenon was temporarily referred to as “seabed fluidization”.

3.1.1 *Before seabed fluidization*

During the consolidation and initial period of wave action, a considerable quantity of tiny bubbles was observed appearing on the seabed surface, venting into the overlying water column (Fig. 3a). This indicated a wave-induced compression effect of seabed skeleton which was essential for pore pressure build-up. During this period, motion of sediments was mostly along the water-seabed interface, as horizontally reciprocating of surface sediments was observed until the water gradually became too turbid to identify the interface. No significant movement of subbottom sediments was detected in this period. Since only waves were simulated in this wave flume (no unidirectional currents), this phenomenon was attributed to the reciprocating wave orbital velocities. Therefore, the SSC increase before seabed fluidization was mainly resulted from the erosion of surface sediments, this opinion was consistent with the finding of Jia et al. (2014).

3.1.2 *After seabed fluidization*

After 3.5 and 2.0 h for the 10 and 15 cm wave rounds respect-

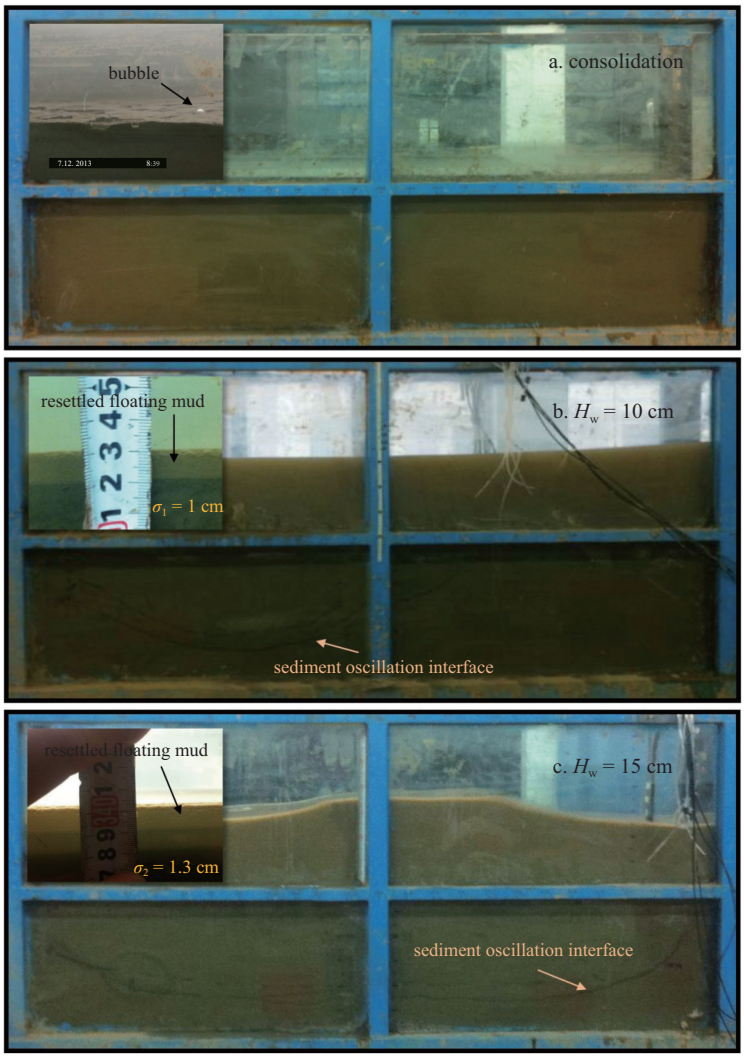

Fig. 3. Side view of the experimental layout. a. In consolidation period before wave action during which tiny bubbles appeared on the seabed surface; b. under 10 cm waves during which seabed shear failure with partial fluidization occurred, after which a floating mud layer of 1 cm in thickness formed; and c. under 15 cm waves during which seabed shear failure with partial fluidization occurred in a larger area, after which a floating mud layer of 1.3 cm in thickness formed.

ively, the SSC reached a steady state (i.e., the first stabilization/the stabilization before fluidization). Subsequently, part of the sediments in shallow layers began to oscillate horizontally along an arc-shaped sub-bottom sliding interface. Meanwhile, sediments were resuspended again until a liquid of higher turbidity formed. There was a significant difference in the shape of fluidized areas in both rounds (Figs 3b and c). In the 15 cm wave round, the horizontal fluidized boundary almost reached the maximum width (≈2.6 m) of the sediment tank; while in the 10 cm wave round, the rightmost fluidized boundary merely slightly beyond the centre (≈1.4 m) of the sediment tank. However, little difference in the fluidized depth was detected (Table 2). In other words, the maximum fluidized area in the 15 cm wave round was almost twice as large as that of the 10 cm wave round. Besides, location of the arc-shaped interface was observed to evolve downwards to the maximum depth firstly and then moved upward to some extent (Xu et al., 2016).

It is worth noting that the initiation of seabed fluidization in the 10 cm wave round was possibly triggered by the disturbance of a core sampler penetration. Because some colleagues who once used this flume argued that 10 cm wave loadings could never liquefy the bottom sediments that had been consolidated for several days. However, this issue was temporarily neglected considering the specific scientific objective in the present study, we believe that as long as fluidization occurred after the first stable state of the SSC, then evaluating the contribution of seabed fluidization to sediment re-suspension makes sense.

Table 2. Parameters of seabed fluidization

H_w/cm	T_b/h	D_{max}/cm	D_f/cm	W_f/cm
10	3.5	34	28	1.4
15	2	36	30	2.6

Note: H_w is the wave height, T_b the time to the initiation of seabed fluidization, D_{max} the maximum fluidization depth, D_f the final fluidization depth, and W_f the maximum width of the fluidized area.

After the termination of wave action and a hydrostatic settlement of suspended sediments for 12 h, a yellow floating mud layer appeared on the seabed surface in both rounds (Figs 3b and c). It is clear that this layer was formed from the redeposition of the suspended materials. Coarse-grained particles deposited faster than the finer ones to mix with the underlying seabed, whereas

fine-grained materials settled down more slowly, to form the floating mud layers on the seabed surface finally.

3.2 *Referenced pore-water pressure*

Attempt was made to record the pore pressure evolutions throughout the two wave rounds in the present study. However, no reliable results were obtained due to some unknown problems of the pore pressure transducers. Fortunately, pore pressure data collected from a similar experiment conducted in the same wave flume in 2015 was available for reference. In order to judge the change of seabed properties resulting from sediment oscillation, the pore pressure records during the corresponding period were referenced (Fig. 4). It is apparent from Fig. 4 that the pore pressure builds up in a short period to offset overlying effective stress, fluidizes the seabed and dissipates over a longer time subsequently. Note that the dramatic build-up of the pore pressure and the initiation of the sediment oscillation were observed to occur almost at the same time, which was a convincing evidence to demonstrate the occurrence of partial seabed fluidization at least.

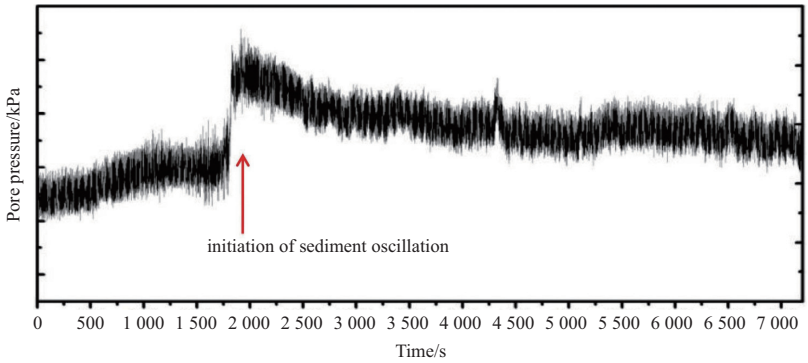

Fig. 4. Referenced pore pressure records during the fluidization period (19:30–21:30 December 21, 2015) in a similar experiment conducted in the same flume. The initiation of seabed fluidization in the 2015 experiment occurred at the same time with the dramatic increase of the pore pressure.

3.3 *Sediment oscillation*

With respect to the phenomenon of the sediment oscillation, some scholars took it as seabed liquefaction directly (e.g., Jia et al., 2014), while some others argued that it was a shear failure of seabed when the wave-induced shear stress exceeded the shear strength of the seabed (e.g., Xu et al., 2006). In this paper, we argued that this kind of sediment oscillation was essentially the combined result of the wave-induced pore pressure build-up and the cyclic shear stress in the seabed. Indeed, the driving force of the sediment oscillation was the shear stress (Fig. 5). However, partial seabed fluidization attenuated the original shear strength to make the wave-induced shear failure easier to occur. In other words, the initiation of the oscillation was resulted from the attenuation of the original shear strength due to the pore pressure build-up (i.e., partial liquefaction). On the other hand, the pore pressure build-up was impossible to approach its overlying effective stress due to the pre-occurrence of sediment oscillation, which significantly increased the seabed permeability and dissipated the pore pressure build-up in time, thus prevented the pore pressure from building up to the final total liquefaction. In this case, the conventional criteria for both "liquefaction" and "shear failure" were not applicable anymore. Shear failure of seabed became easier whereas the total liquefaction of seabed became impossible. Therefore, "liquefaction" was not the most rigorous expression for the the phenomenon of "sediment oscillation" in the present study, so "fluidization" was adopted to indicate the seabed was partially liquefied.

3.4 *Time profiles of SSC*

The occurrence of seabed fluidization was also recorded in the SSC evolutions in both rounds. It is clear in Fig. 6 that the SSCs in both rounds attained two steady states after different periods of wave action: approximately 3.5 h in the 10 cm round and 2.0 h in the 15 cm round for the first stabilization; approximately 11.0 h in the 10 cm round and 8.0 h in the 15 cm round for the final stabilization. Total resuspension load (L_s) showed the same variation trends as those of the SSCs.

The SSC increased with depth in both rounds but the SSC at different depths under 10 cm waves were more uniform than those of under 15 cm waves. This was possibly because the grain

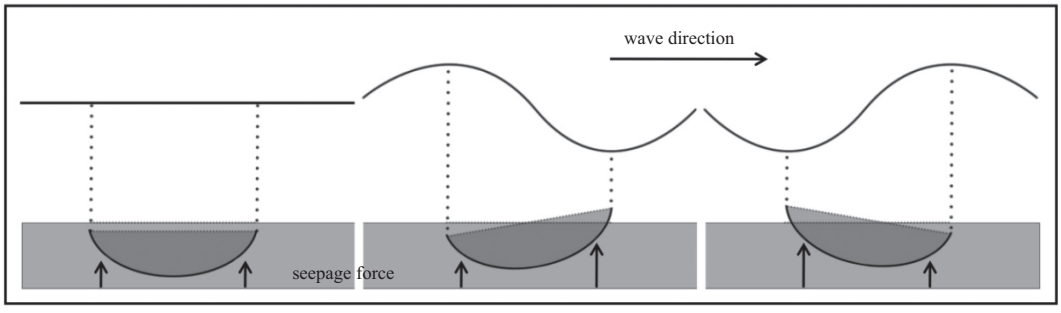

Fig. 5. Schematic mechanism of the wave-induced sediment oscillation (Xu, 2006). The vertical arrows refer to the upward seepage forces acting on overlying sediments, and the horizontal arrows the direction of wave progressing.

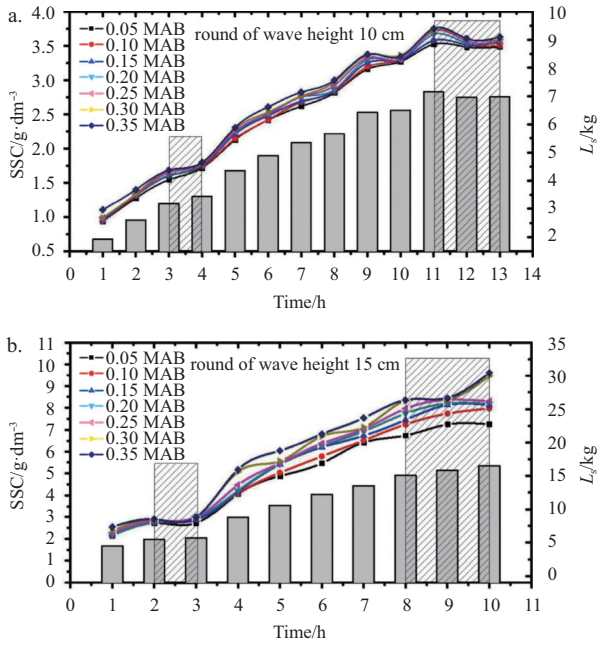

Fig. 6. Time profiles of the SSC at each depth and total suspended load under the 10 cm wave action (a) and those under the 15 cm wave action (b). Note that 0.05–0.35 MAB refers to the elevation of SSC measuring point, meters above the bottom (MAB); latter increase of the SSC in both rounds occurred almost at the same time with the initiation of seabed fluidization (oscillation); and shallow areas represent the stabilized periods of the SSC.

size of suspended materials in the 10 cm wave round was finer with relatively narrow grain size distribution than that of the 15 cm wave round, resulting from the different magnitudes of wave orbital shear stress. In other words, more coarse sediments were suspended into the water column in the 15 cm wave round due to a larger wave orbital shear stress. As coarser sediments were much difficult to be mixed into the upper water layers by the limited convection effect of waves. Therefore, the mixing of sediments between the upper and bottom layers was much easier under 10 cm waves.

4 Discussion

As mentioned previously, the resuspension process in this experiment can be divided into two subphases according to the occurrence of fluidization. Sediment resuspension before fluidization mainly came from the surface of seabed, finally reached the first equilibrium state of the SSC. However, the oscillation of subsurface sediments after seabed fluidization led to the second increase in the SSC and finally reached the second equilibrium state. According to the existing findings and experimental results, the contribution of seabed fluidization to sediment resuspension was preliminarily evaluated via comparing the stabilized resuspension loads before and after fluidization, which was given as

$$C = (M_a - M_b)/M_a, \tag{3}$$

where C is the contribution of fluidization to resuspension; M_b (kg) is the first stabilized total suspended load (i.e., before fluidization); and M_a (kg) is the final stabilized total suspended load (i.e., after fluidization).

The calculated results from the present study were shown in Table 3. Moreover, in order to make a more comprehensive analysis, previously reported results on this issue using both the same flume and sediments were also summarized in Table 3.

4.1 *Quantitative contribution*

The experiments of Jia et al. (2014) and Guo et al. (2016) were also conducted in the same wave flume using similar Huanghe River silts. Different experimental parameters are listed in Table 3. Jia et al. (2014) applied four rounds of waves in sequence over the same seabed, which meant that the experimental condition for each round of the wave height was not single-variable. Therefore, the initial seabed conditions can only account for the sediment behaviors during the first wave round (5 cm wave height). In this case, the results for wave height 7, 10 and 18 cm rounds were merely listed but not employed for discussion. In addition, Jia et al. (2014) divided the two substages according to their self-defined terms namely the initial resuspended increment and the latter re-suspended increment, whereas Guo et al. (2016) and the present study both divided the two substages according to the two stabilized SSC levels. However, this made no difference because the influence of units was ruled out when the contribution was calculated. Besides, Guo et al. (2016) measured the SSC profiles under a single wave height of 15 cm using an instrument for profiling the suspension turbidity in the benthic boundary layer (Argus Surface Meter IV, Argus, Germany), instead of the traditional method of extracting water samples in the present study. However, this also made no difference as long as the accuracy of both measuring methods was assured. Therefore, we believe that the data from Jia et al. (2014) and Guo et al. (2016) are both com-

Table 3. Contribution of seabed fluidization to sediment resuspension

Parameter	Test						
	Jia et al. (2014)	Jia et al. (2014)	Present study	Jia et al. (2014)	Present study	Guo et al. (2016)	Jia et al. (2014)
H_w/cm	5	7	10	10	15	15	18
D/cm	40	40	50	40	50	40	40
T_c/h	2	2	5	2	5	10	2
D_{50}/μm	36–42	36–42	43	36–42	43	43.67	36–42
M_s	2.5/20	3.5/20	4/20	5/20	6/20	7.5/20	9/20
$M_b(M_1)$	0.49	1.55	3314	1.61	5716	2.17	1.70
$M_a(M_2)$	0.18	0.55	6975	0.34	16498	7.05	1.37
C/%	26.9	26.2	52.5	17.4	65.3	76.4	44.6
Use/not	√	–	√	–	√	√	–

Note: The previously reported and present experimental results were summarized for a contrastive analysis. D is the water depth, T_c the consolidation time, D_{50} the median grain size, and M_s the model scale (the ratio of wave height to water depth). In the experiment of Jia et al. (2014), M_1 (kg/m²) is the initial resuspended increment, M_2 (kg/m²) the latter resuspended increment, and M_{max} the maximum quantity of resuspended sediments, thus the contribution was estimated by $C=M_2/M_{max}$.

parable and convincing enough for reference.

The contrastive analysis results were shown in Fig. 7. It is clear that the contribution of fluidization under 10 cm waves (H_w/D=4.0/20.0) reached 52.5% of the total suspension, while the contribution under 15 cm waves (H_w/D=6.0/20.0) accounted for 66.8% in the present study. Such large percentages strongly demonstrated a non-ignorable effect of fluidization on sediment resuspension, seabed fluidization should double the resuspension load under certain conditions. Besides, the contribution seems to be positively correlated with the ratio of the wave height to the water depth. This inference is verified by the previous results because Guo et al. (2016) reported that the contribution exceeds 76.4% under 15 cm waves (H_w/D=7.5/20.0) and Jia et al. (2014) indicated the contribution is approximately 26.9% under 5 cm waves (H_w/D=2.5/20.0). The contribution of fluidization increases with the model scales at a decreasing rate, and the relationship well fits a logarithmic profile which can be expressed as

$$\frac{c_f}{c} = 108.236\ 9 + 26.937\ 01 \ln\left(\frac{H_w}{D} - 0.07\ 606\right), \quad (4)$$

where c_f is the SSC caused by seabed fluidization and c is the total SSC. Temporarily, we believe the decreasing rate resulted from a synchronous increase of resuspension flux due to an enhanced orbital shear erosion from the seabed surface.

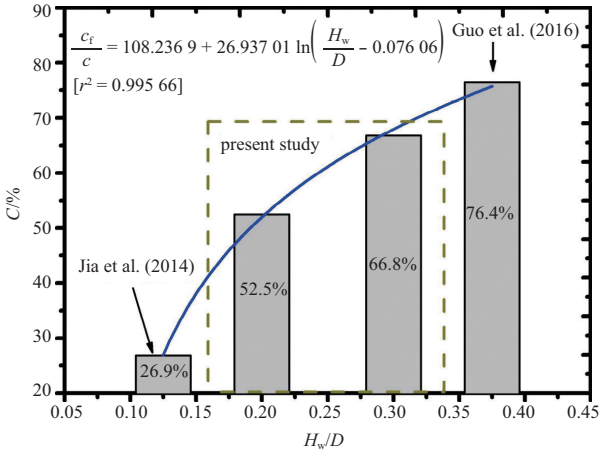

Fig. 7. The contribution of seabed fluidization to the total resuspension under various relative water depth (H_w/D).

4.2 *Physical mechanisms*

As it has been referred before, it was fluidization leading to the second increase of the SSC which could account for at least half of the total suspension. Then what is the physical mechanism for such a great contribution? In the present study, the mechanisms were attributed to two modes for the first time.

The first mechanism is an attenuation of the critical shear stress of surface sediments. It is well known that silt belongs to partially cohesive sediments which always improves the critical shear stress due to the adhesion bond between sediment particles (e.g., Ye, 2012). However, when the seabed was fluidized by waves, attenuation or disappearing of these bonds will surely reduce the critical erosion threshold of surface materials to some extent, and thus more sediments will be eroded (Zhang et al., 2018). In addition, the uplifting seepage forces acting on the surface particles will also help to promoting the entrainment of sediments (Nielsen et al., 2001).

The second mechanism is a hypothesis of subbottom sediment pump action (Zhang et al., 2017) which argues that subsurface fine-grained sediments will be transported from the interior to the surface of a fluidized seabed driven by the upward seepage flows resulting from the wave-induced nonuniform distribution of the pore pressure build up. Because the thickness of the redeposited floating mud materials reached 1.0 and 1.3 cm for the 10 and 15 cm rounds in the present study, respectively, of which the median grain size is only 6.037 μm. It is hard to believe that such a large quantity of fines is all eroded from the water-seabed interface, of which the median grain size is 43.036 μm. Actually, a similar opinion was preliminarily proposed by Tzang (1998) who argued that the wave-induced pore flow acts as piping flows through pore spaces surrounded by solid particle skeletons in the seabed. In weaker regions, very fine soil particles were susceptible to oscillatory seepage flow actions and were easily dislodged from the large-particle skeletons. These detached fine-grained sediments were subsequently suspended in and carried by the pore fluid, which could be defined as “internal sediment suspension”, occurs in any weak pore region inside a seabed, especially with fine-grained constituents. Here in the present study, we developed the hypothesis of Tzang (1998) and argued that detached fine-grained sediments would not only be suspended in the pore fluid, actually, considerable fines could be vertically transported by the pore fluids up to the surface, and easily eroded into overlying water column becoming re-suspended materials, especially when the seabed was fluidized. Strong upward seepage flows in the fluidized seabed and the increased sediment permeability will provide the driving force and preferred paths for seepage pumping of fines, respectively.

The contribution mechanism of the seabed fluidization may have some implications for the future research regarding the resuspension of silty sediments. Because it invalids a commonly-employed opinion that sediments were simply eroded from the surface by the excess of bottom shear stresses to a site-specific critical shear stress of seabed materials. Actually, considerable wave-forced resuspension of silts may have close relationship with seabed fluidization (i.e., pore pressure parameters), because the critical shear stress may be significantly changed by the pore pressures and part of the eroded sediments may originate from the subsurface of seabed.

5 Conclusions

Two rounds of contrast experiment were conducted in a large wave flume with the objective of evaluating the contribution of seabed fluidization to sediment resuspension. The experimental results indicate that seabed fluidization can account for 52.5% and 66.8% of the total suspension under the model scales (H_w/D) of 4.0/20.0 and 6.0/20.0, respectively. Compared with the results of Jia et al. (2014) (C=76.4%, H_w/D=7.5/20.0) and Guo et al. (2016) (C=26.9%, H_w/D=2.5/20.0), a parametric equation for depicting the relationship between the contribution of seabed fluidization and the model scale (the ratio of wave height to water depth) was established. The contribution was found to positively increase with the model scales at a decreasing rate. The physical mechanism of inducing such a large contribution is (1) an attenuation of the critical shear stress for the erosion of surface sediments and (2) a vertical transport of fines driven by the upward seepage flows within the fluidized seabed. We suggest that the future research on the resuspension of silty sediments should pay more attention to the wave-influenced pore pressure parameters.

Acknowledgements

The authors thank Xu Jingping, Liu Hongjun, Xu Guohui, Wang Hu, Guo Lei and Li Hongjiang for their constructive suggestions. Wang Weihong, Li Bowen, Han Chichen, Wang Xiaoqiong, Tang Huiling, Wang Siyu and Ruan Meimei from the Ocean University of China, are acknowledged for their contributions to the experimental campaign and logistic support.

References

Bennett R H. 1977. Pore-water pressure measurements: Mississippi delta submarine sediments. Marine Geotechnology, 2(1–4): 177–189

Bennett R H, Faris J R. 1979. Ambient and dynamic pore pressures in fine-grained submarine sediments: Mississippi Delta. Applied Ocean Research, 1(3): 115–123

Biron P M, Robson C, Lapointe M F, et al. 2004. Comparing different methods of bed shear stress estimates in simple and complex flow fields. Earth Surface Processes and Landforms, 29(11): 1403–1415

Bolaños R, Thorne P D, Wolf J. 2012. Comparison of measurements and models of bed stress, bedforms and suspended sediments under combined currents and waves. Coastal Engineering, 62: 19–30

Bornhold D B, Yang Z S, Keller G H, et al. 1986. Sedimentary framework of the modern Huanghe (Yellow-River) Delta. Geo-Marine Letters, 6(2): 77–83

Clukey E C, Kulhawy F H, Liu P L F, et al. 1985. The impact of wave loads and pore-water pressure generation on initiation of sediment transport. Geo-marine letters, 5(3): 177–183

Danielsson Å, Jönsson A, Rahm L. 2007. Resuspension patterns in the Baltic proper. Journal of Sea Research, 57(4): 257–269

Green M O. 1992. Spectral estimates of bed shear stress at subcritical Reynolds numbers in a tidal boundary layer. Journal of Physical Oceanography, 22(8): 903–917

Green M O, Coco G. 2014. Review of wave-driven sediment resuspension and transport in estuaries. Reviews of Geophysics, 52(1): 77–117

Grant W D, Madsen O S. 1979. Combined wave and current interaction with a rough bottom. Journal of Geophysical Research: Oceans, 84(C4): 1797–1808

Guo Lei, Wen Mingzheng, Shan Hongxian, et al. 2016. Study on resuspension process of seabed sediment induced by wave. Marine Geology & Quaternary Geology (in Chinese), 36(5): 181–188

Jeng D S, Ye J H, Zhang J S, et al. 2013. An integrated model for the wave-induced seabed response around marine structures: model verifications and applications. Coastal Engineering, 72: 1–19

Jia Yonggang, Zhang Liping, Zheng Jiewen, et al. 2014. Effects of wave-induced seabed liquefaction on sediment re-suspension in the Yellow River Delta. Ocean Engineering, 89: 146–156

Kim S C, Friedrichs C T, Maa J P Y, et al. 2000. Estimating bottom stress in tidal boundary layer from acoustic doppler velocimeter data. Journal of Hydraulic Engineering, 126(6): 399–406

Lambrechts J, Humphrey C, McKinna L, et al. 2010. Importance of wave-induced bed liquefaction in the fine sediment budget of Cleveland Bay, Great Barrier Reef. Estuarine, Coastal and Shelf Science, 89(2): 154–162

Mörz T, Karlik E A, Kreiter S, et al. 2007. An experimental setup for fluid venting in unconsolidated sediments: new insights to fluid mechanics and structures. Sedimentary Geology, 196(1): 251–267

Nichols R J, Sparks R S J, Wilson C J N. 1994. Experimental studies of the fluidization of layered sediments and the formation of fluid escape structures. Sedimentology, 41(2): 233–253

Nielsen P. 2002. Shear stress and sediment transport calculations for swash zone modelling. Coastal Engineering, 45(1): 53–60

Nielsen P, Robert S, Møller-Christiansen B, et al. 2001. Infiltration effects on sediment mobility under waves. Coastal Engineering, 42(2): 105–114

Paphitis D, Collins M B. 2005. Sediment resuspension events within the (microtidal) coastal waters of Thermaikos Gulf, northern Greece. Continental Shelf Research, 25(19): 2350–2365

Ross J A, Peakall J, Keevil G M. 2011. An integrated model of extrusive sand injectites in cohesionless sediments. Sedimentology, 58(7): 1693–1715

Saito Y, Yang Zuosheng, Hori K. 2001. The Huanghe (Yellow River) and Changjiang (Yangtze River) deltas: a review on their characteristics, evolution and sediment discharge during the Holocene. Geomorphology, 41(2): 219–231

Seed H B, Rahman M S. 1978. Wave-induced pore pressure in relation to ocean floor stability of cohesionless soils. Marine Geotechnology, 3(2): 123–150

Soulsby R. 1997. Dynamics of Marine Sands. London: Thomas Telford, 249

Sumer B M, Kirca V S O, Fredsøe J. 2012. Experimental validation of a mathematical model for seabed liquefaction under waves. International Journal of Offshore and Polar Engineering, 22(2): 133–141

Tzang S Y. 1998. Unfluidized soil responses of a silty seabed to monochromatic waves. Coastal Engineering, 35(4): 283–301

Tzang S Y, Ou S H, Hsu T W. 2009. Laboratory flume studies on monochromatic wave-fine sandy bed interactions: Part 2. Sediment suspensions. Coastal Engineering, 56(3): 230–243

van Duin E H S, Lijklema L. 1989. The development of an operational two-dimensional water quality model for Lake Marken, the Netherlands. Water Science & Technology, 21(12): 1817–1820

Van Raaphorst W, Malschaert H, Van Harren H. 1998. Tidal resuspension and deposition of particulate matter in the Oyster Grounds, North Sea. Journal of Marine Research, 56(1): 257–291

Wang Y H. 2003. The intertidal erosion rate of cohesive sediment: a case study from Long Island Sound. Estuarine, Coastal and Shelf Science, 56(5): 891–896

Wolanski E, Spagnol S. 2003. Dynamics of the turbidity maximum in King Sound, tropical Western Australia. Estuarine, Coastal and Shelf Science, 56(5): 877–890

Wright L D, Friedrichs C T, Kim S C, et al. 2001. Effects of ambient currents and waves on gravity-driven sediment transport on continental shelves. Marine Geology, 175(1): 25–45

Xu Guohui. 2006. Study on the landslide of gentle-slope silty seabed under waves: a case of the Yellow River Subaqueous Delta (in Chinese) [dissertation]. Qingdao: Ocean University of China

Xu Guohui, Liu Zhiqin, Sun Yongfu, et al. 2016. Experimental characterization of storm liquefaction deposits sequences. Marine Geology, 382: 191–199

You Zaijin. 2005. Fine sediment resuspension dynamics in a large semi-enclosed bay. Ocean Engineering, 32(16): 1982–1993

Yuan Ye, Wei Hao, Zhao Liang, et al. 2009. Implications of intermittent turbulent bursts for sediment resuspension in a coastal bottom boundary layer: a field study in the western Yellow Sea, China. Marine Geology, 263(1): 87–96

Ye Jianhong. 2012. 3D liquefaction criteria for seabed considering the cohesion and friction of soil. Applied Ocean Research, 37: 111–119

Zhang Shaotong, Jia Yonggang, Guo Lei, et al. 2016a. In-situ observation of sediment deposition process in Chengdao sea area of the Yellow River estuary. Marine Geology & Quaternary Geology (in Chinese), 36(3): 171–181

Zhang Shaotong, Jia Yonggang, Liu Xiaolei, et al. 2016b. Feature and mechanism of sediment dynamic changing processes in the modern Yellow River Delta. Marine Geology & Quaternary Geology (in Chinese), 36(6): 33–44

Zhang Shaotong, Jia Yonggang, Wen Mingzheng, et al. 2017. Vertical migration of fine-grained sediments from interior to surface of seabed driven by seepage flows-"sub-bottom sediment pump action". Journal of Ocean University of China, 16(1): 15–24

Zhang Shaotong, Jia Yonggang, Zhang Yaqi, et al. 2018. Influence of seepage flows on the erodibility of fluidized silty sediments: parameterization and mechanisms. Journal of Geophysical Research: Oceans: doi: 10.1002/2018JC013805